Design and Implementation of a Mechanical Control System for the Scanning Microwave Limb Sounder

William Bowden *
The University of British Columbia, Vancouver, BC, V5L 2T7, Canada

February 8, 2011

Abstract

The Scanning Microwave Limb Sounder (SMLS) will use technological improvements in low noise mixers to provide precise data on the Earth's atmospheric composition with high spatial resolution. This project focuses on the design and implementation of a real time control system needed for airborne engineering tests of the SMLS. The system must coordinate the actuation of optical components using four motors with encoder readback, while collecting synchronized telemetric data from a GPS receiver and 3-axis gyrometric system. A graphical user interface for testing the control system was also designed using Python. Although the system could have been implemented with a FPGA-based setup, we chose to use a low cost processor development kit manufactured by XMOS. The XMOS architecture allows parallel execution of multiple tasks on separate threads–making it ideal for this application and is easily programmed using XC (a subset of C). The necessary communication interfaces were implemented in software, including Ethernet, with significant cost and time reduction compared to an FPGA-based approach. For these reasons, the XMOS technology is an attractive, cost effective, alternative to FPGA-based technologies for this design and similar rapid prototyping projects.

Nomenclature

I_v	Radiative Intensity
s	Distance of from detector
α	Absorption Coefficients
S	Radiative Source
ν	Frequency

*USRP Intern, Jet Propulsion Laboratory, 4800 Oak Grove Drive, Pasadena, CA

k	Boltzmann constant
T	Temperature
T_b	Brightness Temperature
$\tau(s)$	Optical Depth Function
n	Number of Threads

1 Introduction

The effects of change in atmospheric composition is one of the critical issues facing the scientific community. In order for researchers to address these issues, it is important they have access to accurate data concerning the concentrations of key chemical species in our atmosphere. Following on previous Earth observing missions such as the Upper Atmosphere Research Satellite and the Aura Satellite, the Scanning Microwave Limb Sounder (SMLS) will make use of new technological developments to provide improved global coverage and resolution of the atmosphere. This project outlines the design and implementation of a control system which will be used in the high altitude testing of the SMLS prototype.

1.1 Remote Sensing Using Thermal Emission

One remote sensing technique utilizes the thermal emission properties of molecules and radiative energy transfer physics to determine chemical composition of the atmosphere. Fundamentally, the radiative intensity, I_v, is governed by three effects: enhancement of energy due to emission, energy loss due to absorption and a redistribution of energy due to scattering. If scattering effects are neglected, the following differential equation governs the intensity:

$$\frac{dI_v}{ds} = -\alpha I_v + S \tag{1}$$

where α is the absorption coefficient and S is the source term. For atmospheric applications one can assume thermal equilibrium and the source term can be described using the Planck's equation for black body radiation.

$$B(T) = \frac{2h\nu^3}{c^2} \frac{1}{e^{\frac{h\nu}{kT}} - 1} \tag{2}$$

Using Planck's formula, the differential expression in equation 1 has the following solution:

$$I_v(0) = I_v(s_0)e^{-\tau(s_0)} + \int_0^s B(T)e^{-\tau(s')}\alpha ds' \tag{3}$$

where the first term accounts for the boundary radiation at a distance s_o and the second term is from the thermal emission integrated over the travel path. T is the spatial temperature and the microwave detector is, by convention, at the origin. τ is the optical depth function and is defined as:

$$\tau(s) = \int_0^s \alpha(s')ds' \tag{4}$$

However, in the microwave regime, where $hV \ll kT$, Planck's equation becomes a linear relationship between temperature and brightness:

$$B(T) \approx \frac{2\nu^2 kT}{c^2} = \frac{2kT}{\lambda^2} \tag{5}$$

For this reason, results are often normalized to express brightness in units of brightness temperature T_b. Using this approximation, equation 3 can be re-expressed in terms of T_b as:

$$T_b(0) = T_{b0}e^{-\tau(s_0)} + \int_0^s T(s')e^{-\tau(s')}\alpha ds' \tag{6}$$

The forward calculation answers the question "given the chemical composition which affects the absorption coefficient and the temperature profile, what brightness do I expect to measure?" For remote sensing we are interested in the inverse question,"given that I detect a certain spectral brightness, what atmospheric properties reside in the integral?" The details of answering this question are highly complex and outside the scope of this report. It involves looking at molecules, such as O_2, with known chemical concentrations to determine pressure and temperatures, while using correlation and fitting algorithms to match spectral features to atmospheric constituents. The results of answering this question can be seen in the following figure.

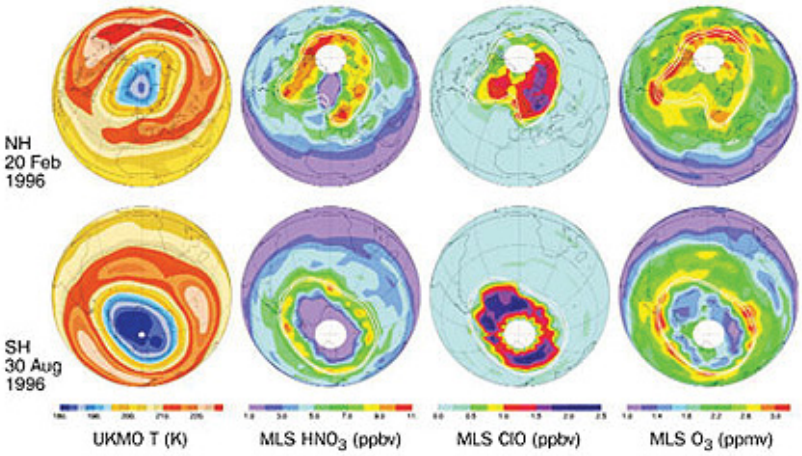

Figure 1: Chemical concentration profiles of various atmospheric species.

1.2 Scanning Microwave Limb Sounder

The Microwave Limb Sounder will make use of technological advancements in superconducting heterodyne mixers to provide atmospheric data with high spectral resolution. The mixer modulates the incoming RF signals with a local oscillator (LO), resulting in an output signal with a frequency equal to the difference of the RF and LO frequencies and power proportional to the thermal emission. With a lower frequency, the atmospheric signal is more easily filtered and amplified. Next, the signal is analyzed using a digital polyphase spectrometer. This system, along with the optical front end and calibration references are shown in Figure 2:

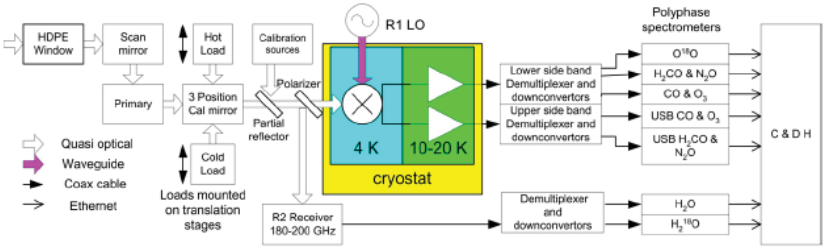

Figure 2: Diagram of the SMLS system.

The system will soon be ready to be tested. There will an airborne test flight to provide important feedback on the capabilities of the device. The prototype airborne SMLS instrument, A-SMLS, will fly on the WB-57 aircraft at altitudes between 15 to 17 km where it will collect a limb view covering 200 km of cross-track scan. The key parameters of the SMLS are listed in Table 1.

Table 1: Key system properties of the SMLS

Parameter	Value	Notes
Antenna aperture	20 cm	Required for 2 km vertical resolution at 200 km
Azimuth scan period	47 s	Dictated by 10 km horizontal resolution
Elevation scan period	2 s	Dictated by 12.6 km/minute air speed
Azimuth scan range	±30°	Provides 200 km horizontal scan at tangent point
Elevation scan range	4°	Provides 10 km vertical scan for allowing for 1° pitch variation
Vertical scans per horizontal scan	20	Dictated by 10 km horizontal resolution and 200 km scan width
Integration time	100 ms	Provides 1 km vertical resolution

1.3 Mechanical Control System for the A-SMLS

A control system for these tests is needed to coordinate the A-SMLS's optical components necessary for collecting thermal emissions and synchronizing data with the detector's spatial location and orientation. This includes defining the atmospheric scan paths, regulating the sampling of radiometric refernce (calibration) views, and recording telemetric data from a GPS receiver and three axis gyro packages. Section two of the report provides an overview of all the system components. Section three details the implementation of the control system in software.

2 Design Overview of the A-SMLS Control System

The control system consists of four motors which actuate the various optical components along with telemetric data receivers required to synchronize atmospheric data with the wing pod's location and spatial orientation. This section provides an overview of the functionality of these components. A block diagram with the communication system is shown in the following figure.

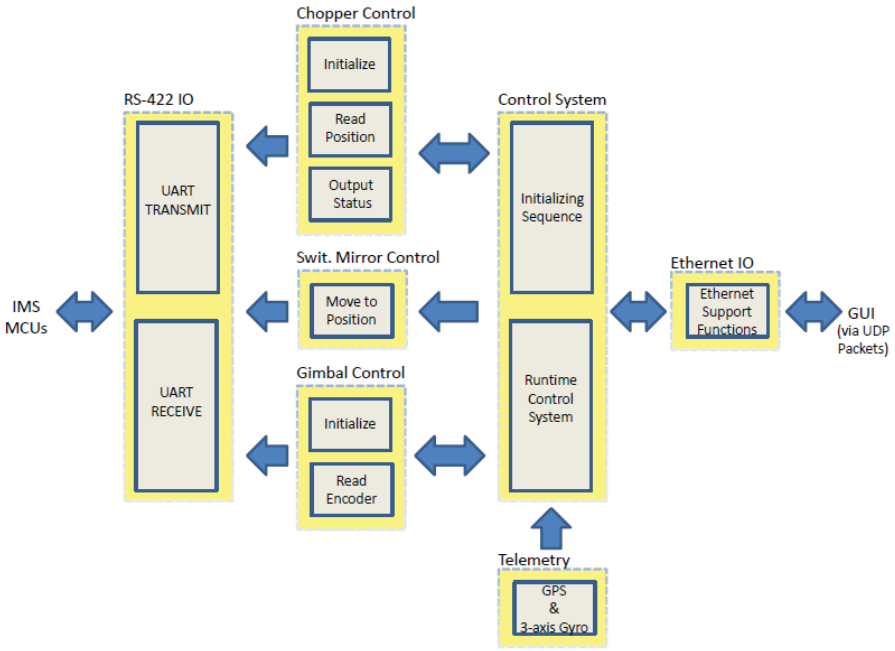

Figure 3: Block diagram showing the operation of the control system with IO systems.

2.1 Two Axes Scanning Gimbal

The atmospheric measurement swaths are traversed using a two axis gimbal, one axis to scan over elevation and the other to scan over the azimuth angle, with single ended quadrature encoder feedback. The device has set optical limits restricting angular rotation for each axis to prevent mechanical interference with other components in the instrument.[1] The gimbal was custom manufactured by Newmark Systems and is shown in the following figure.

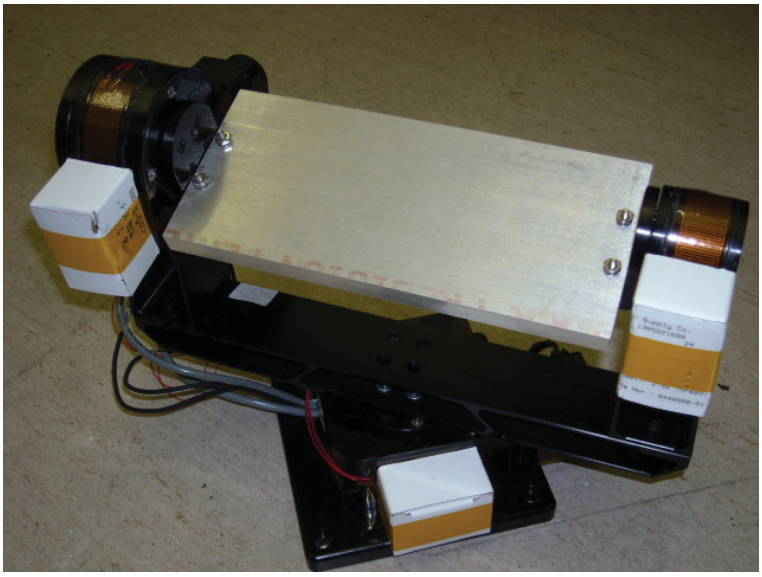

Figure 4: Newmark Systems' two axis gimbal.

In the final design for the wing pod, a reflective mirror will be mounted to the gimbal to reflect thermal emissions from the window to the radiometer. A custom closed loop feedback system was designed to precisely control the gimbal's position and a detailed description of the algorithm is covered in section 3.4. If a move command is sent to the gimbal before the previous scan has completed, an error message will be generated. The atmospheric limb scan cycle with calibration reference measurements is shown in Figure 5.

2.2 Switching Mirror

The raw spectral data from the radiometer must be processed into the concentration of the various atmospheric constituents. This requires calibrating the device using two reference targets, an ambient temperature microwave absorbing target and a view towards deep space. The switching mirror is mounted to

[1] The optical limits had to be reversed because the gimbal limits are active high while the MCU's have active low limit detection.

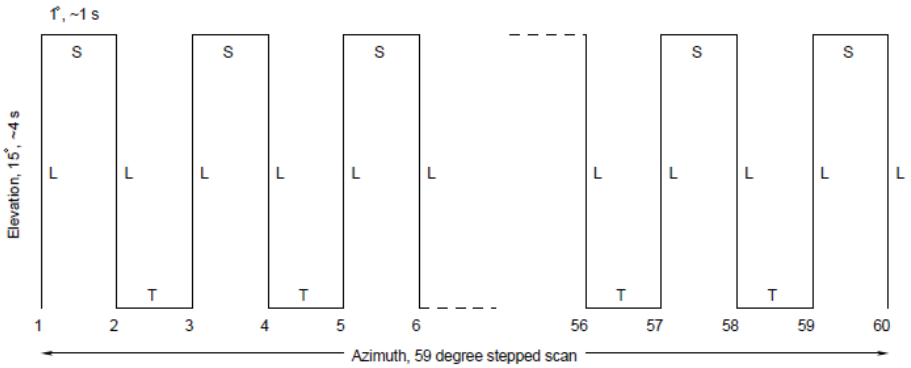

Figure 5: The scan path of the SMLS is shown with the sampling of the reference target(T), a space view (S), and the limb (L).

a stepper motor manufactured by Schneider Electronics. Commands are sent to the MCU controller to set the mirror at precise angles that reflect emission from either the primary mirror or one of the two radiometric reference views. This configuration can be seen in Figure 6. The reference and atmospheric data are interpolated together to calibrate the scientific measurements. This interpolation introduces systematic noise into the measurements which decreases with the amount of reference samples and regularity in distribution with respect to atmospheric measurements. However, a trade off is made since increasing reference measurements reduces the amount of collected scientific data.

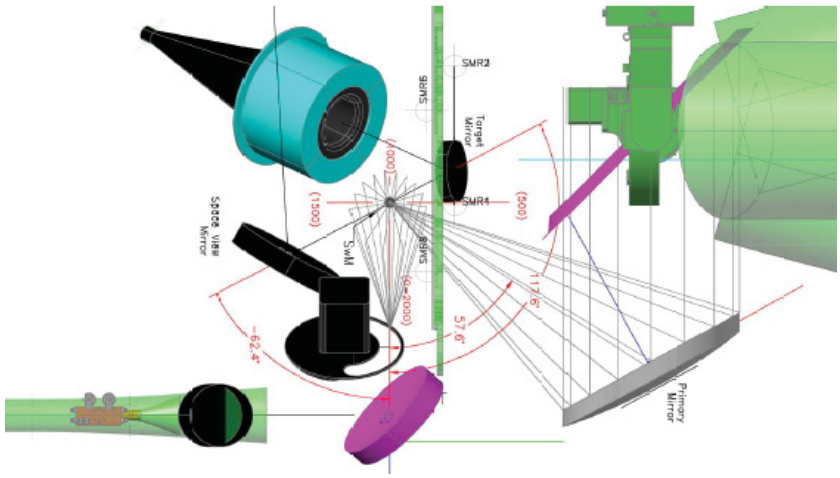

Figure 6: Alignment of the optical components of the SMLS.

2.3 Rotary Chopper

The electronic system exhibits fluctuations in the gain. To compensate for this systematic error, we provide a periodic reference signal using a rotating chopper in the beam path. It is located between the switching mirror and the mixer receiver such that all collected signals must pass through the chopper before being processed. The chopper consists of two parts, a through hole which allows the atmospheric signal to pass through unattenuated and a microwave absorber. The device is shown in Figure 7. The chopper rotates at a steady rate of 10+/-.002 Hz. The absorber has characteristic emission properties over the microwave regime and provides a known signal for calibration. Gain drifts can be accounted for in the data rapidly switching between absorber reference and signal.

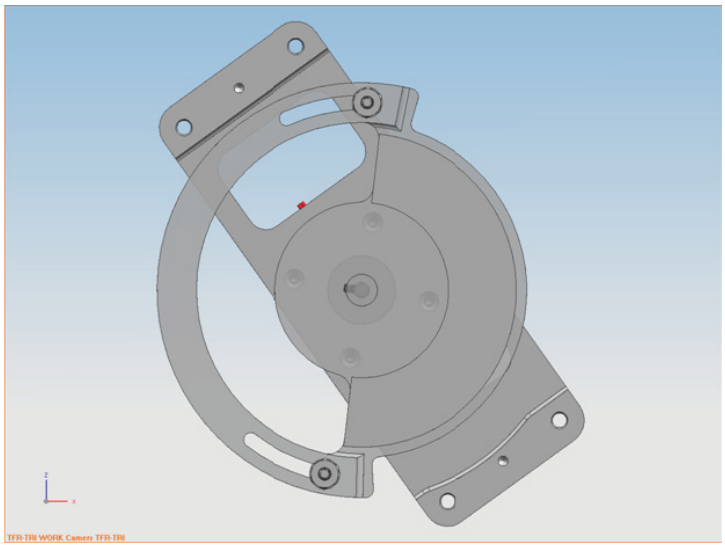

Figure 7: The rotary chopper.

The chopper serves a secondary purpose with respect to the control system's design by providing a steady signal to synchronize simultaneous events. The IMS MCU outputs an index mark once per cycle. All events are executed in terms of index marks, e.g. one azimuth scan is 40 index marks–approximately 4 seconds. This has the benefit over a time based system by preventing a desynchronization between chopper rotations and scan swatches. For post experiment data processing, having a different number of absorber/atmosphere data pair measurements per scan adds complication. This is eliminated by ensuring that every scan starts on an index mark, has a duration less than an integer number for chopper periods, and begins again at the next index mark after the switching mirror is stable.

2.4 Telemetry

The control system includes a GPS receiver and a three axis gyro package. The GPS data will match chemical composition data with the device's atmospheric position. Atmospheric data is also affected by the angle of the scan path, which is corrected for by the three axis gyro package.

2.5 Control System States

The control system design consists of three states: initialization, data acquisition, and stop. The initialization sequence consists of powering up the chopper until it stabilizes at the desired rotational velocity. Next, the two gimbal axes are moved to their negative limits and then moved forward one index mark. Finally, the switching mirror is set to the limb view for the first scan. This process is shown graphically in Figure 8.

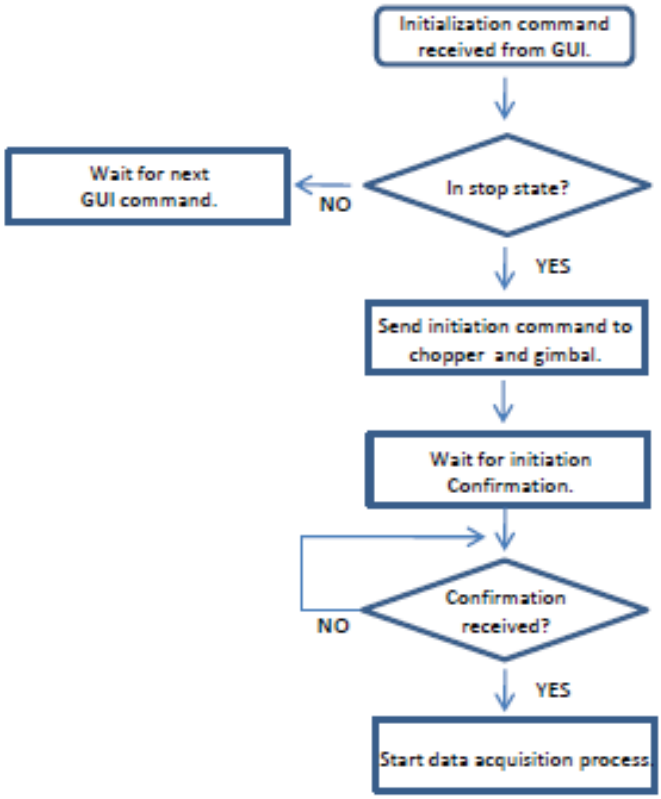

Figure 8: Flowchart showing the initialization sequence of the control system.

The data acquisition process consists of counting the index marks and determining what the correct response is given the state of the system. This includes controlling the gimbal and setting the mirror position. Also, telemetric data is collected and outputted to a host computer at set data rates. This process is also shown graphically in Figure 9. The stop state puts the system into idle and waits for the initialization command.

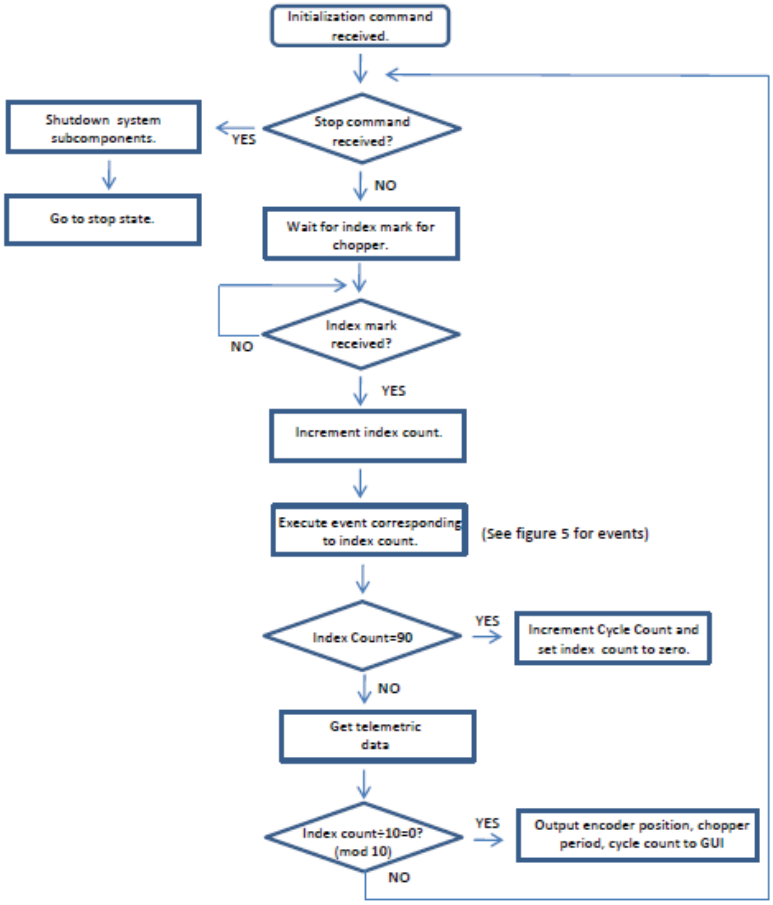

Figure 9: Flowchart showing the data acquisition process of the control system.

3 Implementation of the A-SMLS Control System

The mechanical control system was implemented using the XC-2 development board manufactured by XMOS. The XMOS device was chosen over a FPGA

driven system based on cost and time considerations. The XMOS architecture allows parallel event driven applications on multiple threads, while being programmable using XC (a real-time subset variant of C).

3.1 XMOS Processors

At a cost of $150, the XC-2 development kit is an attractive choice for synchronized, real time, event driven applications. When compared to an equivalent FPGA-based approach, an XMOS processor has significant advantages in both cost and programming simplicity. The XMOS is based on the Transputer microprocessor architecture developed in the 1980's for parallel computing which is being revamped in this new platform. The XMOS device has multiple cores capable of running parallel applications on separate threads. The threads communicate with each other via user defined channels capable of transmitting data within the device. XMOS guarantees the processing speed of n threads to be:

$$processor\ speed = \begin{cases} 100\ MIPS & n \leq 4 \\ \frac{400\ MIPS}{n} & n > 4 \end{cases} \tag{7}$$

where n is the number of current threads. XMOS has coined their technology "Software Defined Silicon" because of its ability to implement low-level I/O in software. They provide their own C-based development environment using XC which eliminates the need for custom tool kits associated with FPGA programming. The XC-2 has four cores and necessary hardware for Ethernet I/O. The XMOS device and interfacing board are shown in Figure 10.

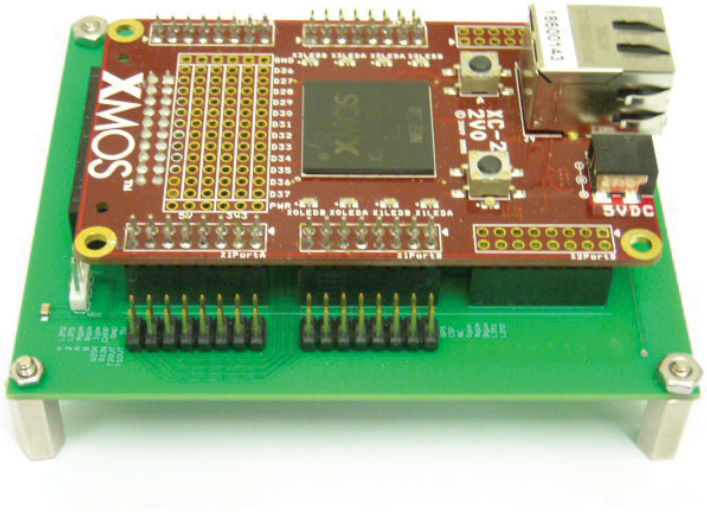

Figure 10: The XMOS XC-2 board with communication interfacing board.

3.2 XMOS Interfacing Board

The XMOS board was required to interface with various system subcomponents. This includes a two serial connection, a RS-422 for the MCUs and RS-232 for the gyro package, requiring two transceivers manufactured by Maxim IC (MAX3070E, MAX13234E). It was decided what processor cores would control specific systems since each I/O pin can only be accessed on a single specified core. The schematic of the board can be seen in appendix 1. Table 2 lists all I/O ports with their physical addresses. The GPS unit uses TTL logic levels and can be directly routed to the board. The board also has 5V input to power the XMOS board.

Table 2: I/O Ports of the XMOS Interfacing Board

Component IO	Hardware Address
Limit+ Gimbal X	X1d11
Limit- Gimbal X	X1d10
A,B Encoder Gimbal X	X1d6 to X1d9
Index Gimbal X	X1d1
Index Chopper	X1d0
Limit+ Gimbal Y	X1d13
Limit- Gimbal Y	X1d12
A,B Encoder Gimbal Y	X1d18-X1d21
Index Gimbal Y	X1d23
Transmit RS-422 (MCUs)	X3d13
Receive RS-422 (MUCs)	X3d12
Transmit 1 RS-232 (Gyro)	X3d0
Receive 1 RS-232 (Gyro)	X3d1
Transmit 2 RS-232 (free)	X3d22
Receive 2 RS-232 (free)	X3d23
GPS	X3D11
Spare 4 bit Port	X3d2-X3d5
Spare 4 bit Port	X3d6-X3d9

The surface mount PCB board was designed using EagleCAD, an open source electrical design program capable of making simple surface mount boards.

3.3 IMS Motor Control Units

All four of the system's stepper motors are controlled using Motor Control Units (MCU) manufactured by Intelligent Motor Systems. The MCU, shown in figure 11 have integrated index, driver and encoder feedback with the ability to program acceleration/deceleration rates, encoder resolution and power output. Also, it is possible to operate multiple controllers on the same RS-422 port by assigning a single ASCI character name to each device. In multi-device or party mode, a MCU will respond only to commands which begin with their name and

end with the linefeed character. However, once in party mode, devices cannot be prompted to return state information such as encoder position or operational parameters. The IMS controllers were also tuned to optimize parameters such as settling time of switching mirror, velocity of the gimbal and power consumption of all the motors. These parameters are listed in Table 3.

Table 3: IMS Motor Parameters

Motor	Hold/Run Current Final Vel.	Accel./Decel. Deadband	Init. Vel.
Chopper	5/15 1500	10/10 disabled	400
Mirror	5/65 15170	5/10 disabled	15170
Gimbal X	5/15 3000	10/10 disabled	400
Gimbal Y	5/15 3000	10/10 disabled	400

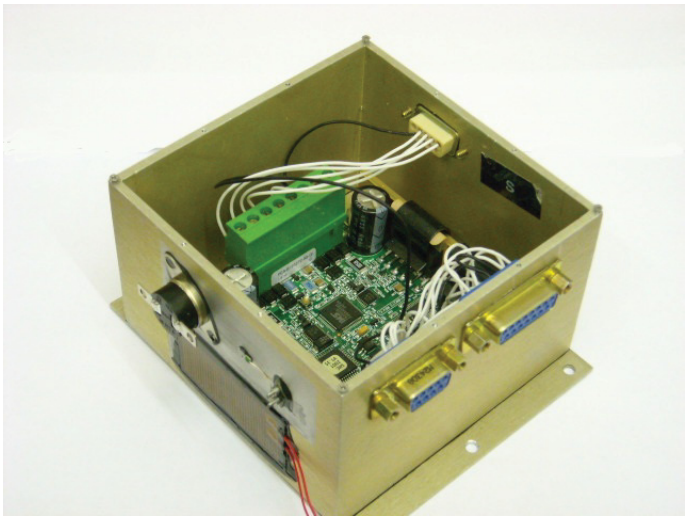

Figure 11: A MCU manufactured Intelligent Motor Systems.

3.4 Quadrature Encoders

All four of the motors used in the system have differential encoder feedback for precision control of angular position. We need position feedback of the gimbal to synchronize the radiometer data with the scanning mirror angle. Therefore, using the IMS controller in party mode to get position is not possible because

there is no read back command. Instead, an encoder control system was implemented in software using the XMOS card. A differential encoder consists of two quadrature square wave signals–typically referred to as A and B–which are outputted as the motor shaft rotates. This can be seen in Figure 12.

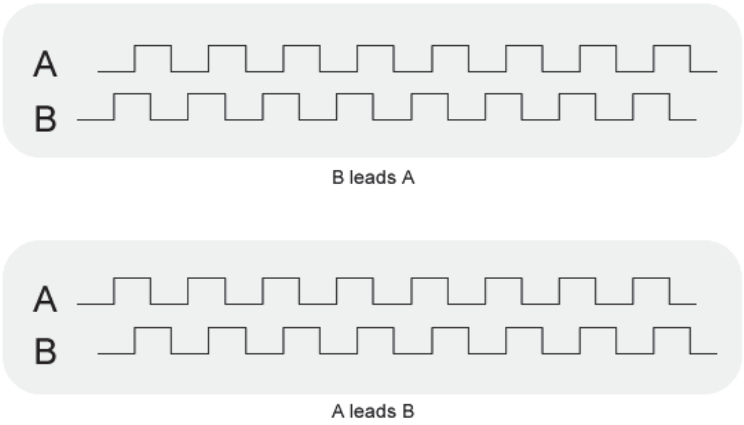

Figure 12: Output signals of a quadrature encoder.

By reading the values of A and B as the shaft rotates one can determine the direction of rotation, e.g. if A,B=01,11,10,00... corresponds to clockwise then A,B=10,11,01,00... is counter clockwise, and the frequency of transitions gives motor velocity.

Initially, the AB value was sampled by the XMOS device when a transition occurred and compared to the previous state. The XMOS processor has the ability to only sample the encoder input when a change is detected-saving CPU cycles. However, the quadrature signals exhibit instability as the motor accelerates and decelerates as it transitions between states, which can lead to signal 'bounce' and false encoder readings. This results in accumulative errors in the azimuth position which is traversed using multiple short scans.

A more accurate technique is to wait for a transition on either A or B, then read the other quadrature signal to determine the direction of rotation. Once a transition is detected, it should be re-sampled in quick succession to ensure the signal is not system noise. Continue to repeat this loop, alternating between the A and B edges until the desired position is reached. A detailed explanation of the algorithm is given in Figure 13. To verify the XMOS encoder's operation, a single IMS controller was used to sweep the gimbal back and forth over a set angle at three different speeds for 1 hour. As the angle was rotated the IMS position readout was compared to the XMOS encoder value.

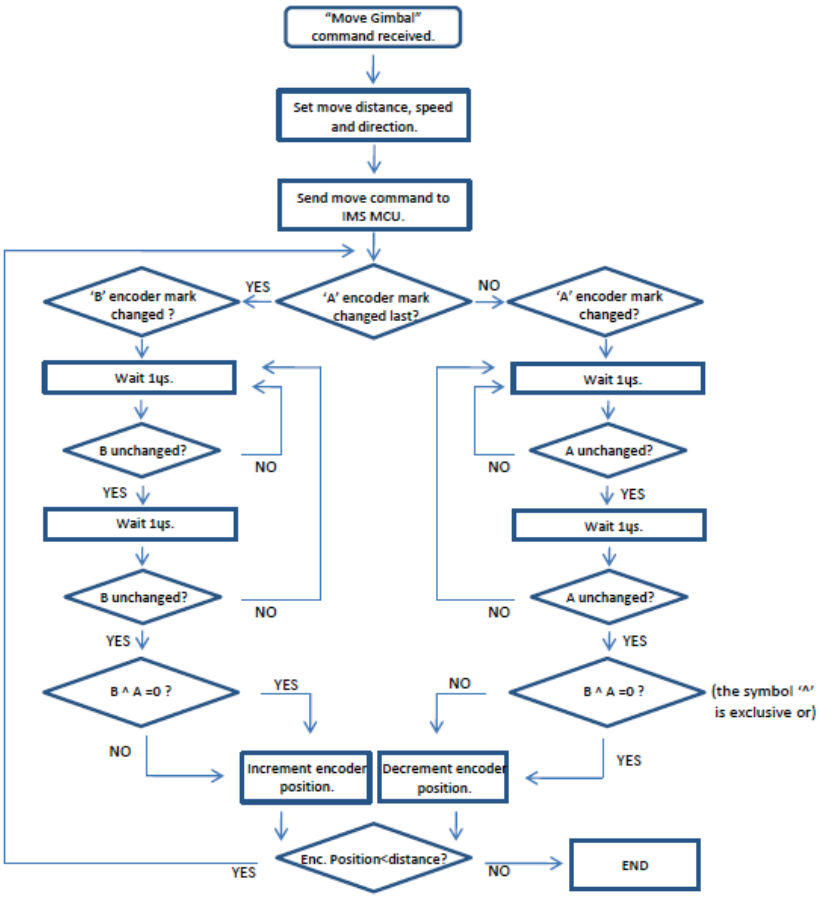

Figure 13: Flowchart of the gimbal encoder control algorithm.

3.5 Python GUI

To test the control system a graphical user interface (GUI) was designed using PyQt4, a development suit for creating GUIs in Python. PyQt4 allows the user to design the GUI graphically by placing objects such as dialogue boxes, drop down menus, push buttons and other IO components and generates the associated Python code during compilation. PyQt4 also allows for the embedding of Matplotlib objects for plotting data. The GUI is shown in Figure 14. The GUI connects to the XMOS board via Ethernet and has multiple parallel threads to handle data input, command/dialog IO, data plotting, and measurement reading. The GUI is capable of plotting the angle of both gimbal axes, the chopper frequency, and mirror position. It allows the user to send start, stop and reinitialize commands to the XMOS device. The progress of the current scan is monitored along with the total number of scans completed.

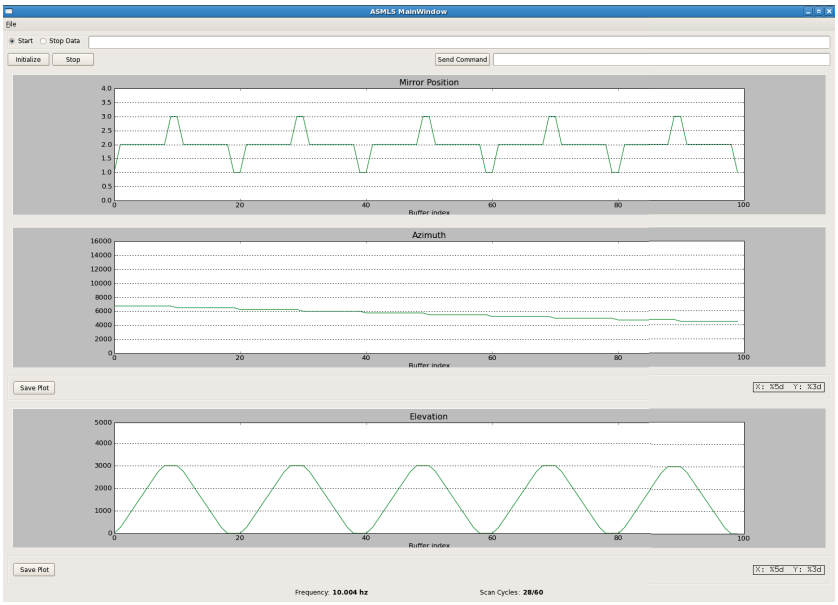

Figure 14: Graphical user interface for the control system.

4 Future Design Modification and Recommendations

Precise calibration of certain system subcomponents was not possible since they are currently unavailable. The chopper attachment for the motor shaft has yet to be manufactured and the mirror for the gimbal is currently being used by the mechanical team. Once the chopper is available it should be mounted to the shaft and various time constants must be measured. The time necessary to accelerate to an angular velocity of 10 Hz must be determined for the initialization process. Also, the times between the index marks to the chopper "though hole" and the chopper "through hole" to the absorber must be measured. Currently, there is a four bit port that outputs these period signals as a square wave which can be used for calibration. The chopper state must be outputted with data packets for calibration. Once the scan mirror is availed, the IMS scan parameters for the gimbal in both the azimuth and elevation direction must be reset.

Secondly, the Ethernet connection between the XMOS board and the host data logging computer is based on example source code provided by XMOS. The code has both transmit and receive functions operating on the same thread. However, the sample code is implemented to stall as it waits for incoming UDP messages. I accounted for this issue by the host computer returning a confirmation message whenever a data packet is received. I attempted to put the transmit and receive Ethernet protocols on separate threads so the two tasks

are independent, however the program would stall whenever a transmit was attempted. It may be beneficial to further investigate this issue since a solution would simplify implementing Ethernet IO in future projects.

One minor change should be implemented if the interface board is remanufactured. The two 4-bit ports (XMOS ports are either 1, 4, 8 or 16 bits) which reads both of the gimbal encoders should have the AB signals as the two least significant bits. I misread the data sheet and put A and B on two middle bits which adds complexity when sampling the port.

5 Conclusion

I have designed and implemented a control system capable of synchronizing the various subcomponents of the SMLS. Using an XMOS processor the design was implemented entirely in software. This eliminated the need for a more complex FPGA-based system which would have increased the time, cost and complexity of the project. This project also serves as an example for capabilities of the XMOS device for real-time event driven applications. Furthermore, much of the code, such as the communication system, can be reused on future projects. The functions of various subsystems were outlined and their interactions with the other components for the proper operation of the SMLS were addressed. Using a GUI programmed in Python, the sub system was tested to ensure proper operation.

6 Acknowledgements

I would like the thank NASA Undergraduate Student Research Program for giving me the opportunity to work at Jet Propulsion Laboratory. It has been an excellent learning experience and helped me develop my future career goals. I would like to acknowledge Robert Jarnot, Paul Stek and the MLS group for their guidance and support during my internship. I feel truly privileged to have had the opportunity to work in this outstanding community with such talented engineers and scientists.

This research was carried out at the Jet Propulsion Laboratory, California Institute of Technology and was sponsored by the National Aeronautics and Space administration and the NASA Undergraduate Student Research Program.

Appendix A: Circuit Schematic for XMOS Interfacing Board

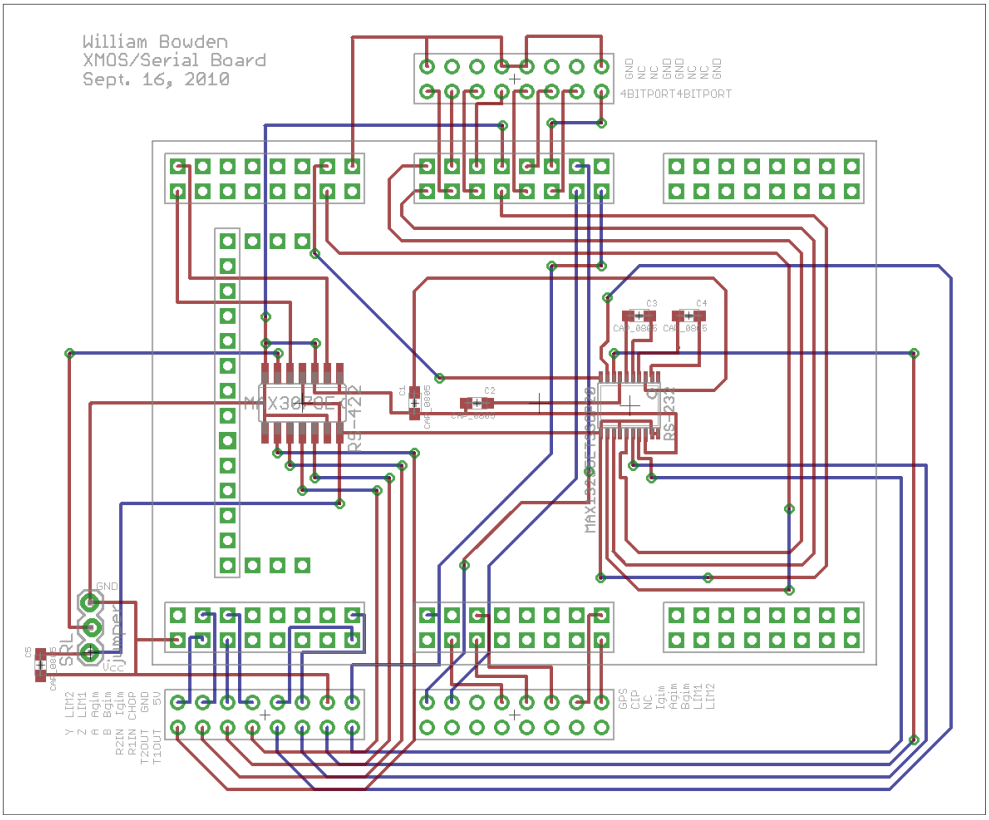

Figure 15: Surface mount board design onto which the XMOS XC-2 card is mounted.

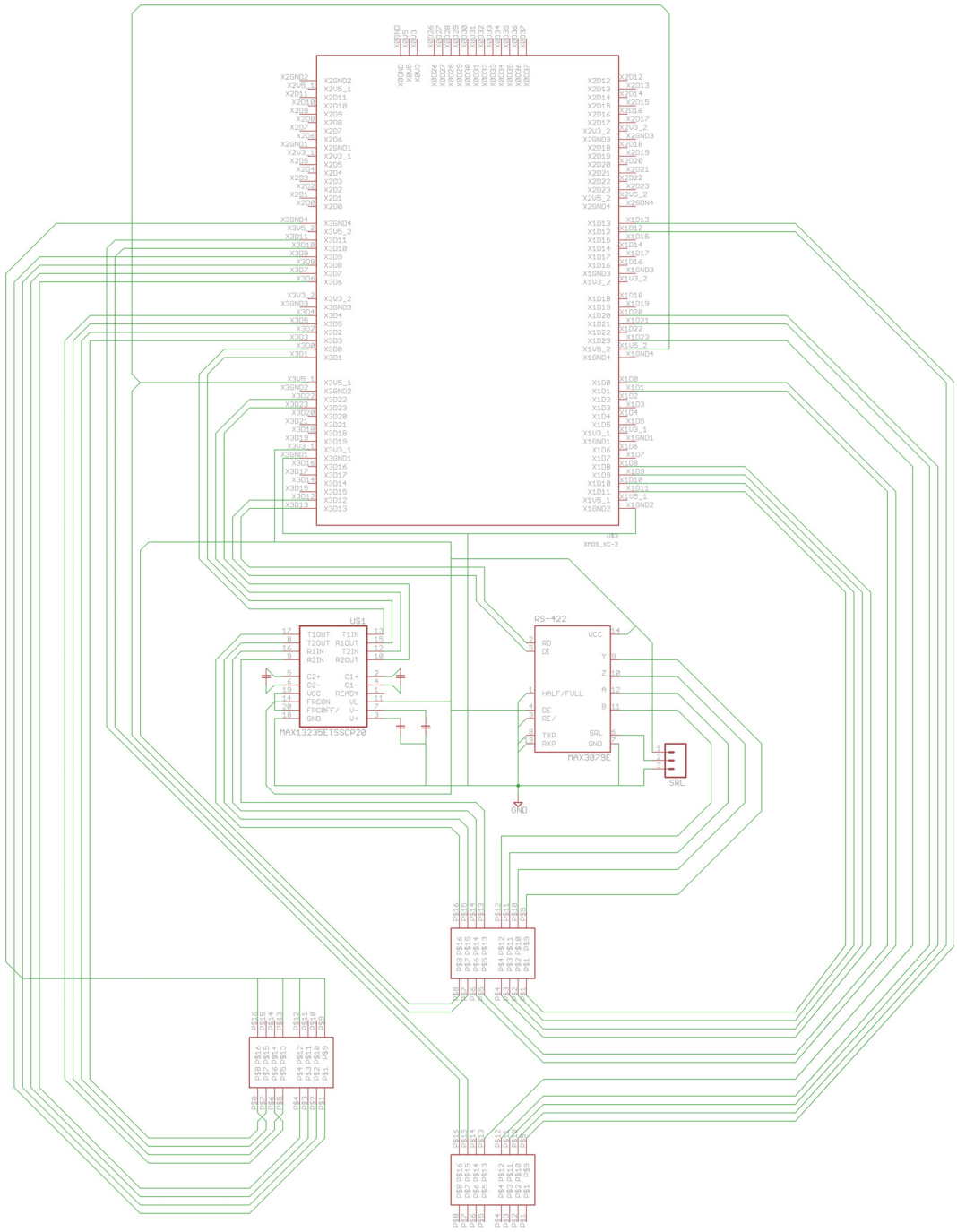

Figure 16: Schematic for serial/PCB board.

References

[1] Robert F. Jarnot et. al., *Radiometric and Spectral Performance and Calibration of the GHz Bands of EOS MLS*. IEEE Trans. Geosci. Remote Sens., Vol. 44, No. 5, pp. 1075 1092, May 2006.

[2] F. Rice et al., *SIS mixer design for a broadband millimeter spectrometer suitable for rapid line surveys and redshift determinations*. Proc. SPIE Int. Soc. Opt. Eng., Vol. 4855, pp. 301-311, Feb. 2003.

[3] John S. Ward et. al., *SIS mixer design for a broadband millimeter spectrometer suitable for rapid line surveys and redshift determinations*. Proc. SPIE Int. Soc. Opt. Eng., Vol. 4855, pp. 301-311, Feb. 2003.

[4] Leslie Lamport, *Sensitive Broadband Receivers for Microwave Limb Sounding*. Jet Propulsion Laboratory.

[5] J. W. Waters et al, *The Earth Observing System Microwave Limb Sounder (EOS MLS) on the Aura Satellite*. Proc. SPIE Int. Soc. Opt. Eng., Vol. 4855, Vol. 44, No. 5, pp. 1075 1092, May 2006.

[6] Dr. Paul Stek, Private Communications. August-December 2010.

[7] Dr. Robert Jarnot, Private Communications. August-December 2010.